Mechatronics 24 (2014) 87–97

Contents lists available at ScienceDirect

Mechatronics

journal homepage: www.elsevier.com/locate/mechatronics

Robust PID control of fully-constrained cable driven parallel robots

Mohammad A. Khosravi *, Hamid D. Taghirad

Advanced Robotics and Automated Systems (ARAS), Industrial Control Center of Excellence (ICCE), Faculty of Electrical and Computer Engineering, K.N. Toosi University of Technology, Tehran, Iran

ARTICLE INFO

Article history:
Received 24 December 2012
Accepted 8 December 2013
Available online 4 January 2014

Keywords:
Cable driven parallel robot
Dynamical uncertainties
Robust PID control

ABSTRACT

In this paper dynamic analysis and robust PID control of fully-constrained cable driven parallel manipulators are studied in detail. Since in this class of manipulators cables should remain in tension for all maneuvers in their workspace, feedback control of such robots becomes more challenging than that of conventional parallel robots. In this paper, structured and unstructured uncertainties in dynamics of the robot are considered and a robust PID controller is proposed for the cable robot. To ensure that all cables remain in tension internal force concept is used in the proposed PID control algorithm. Then, robust stability of the closed-loop system with proposed control algorithm is analyzed through Lyapunov direct method and it is shown that by suitable selection of the PID controller gains, the closed-loop system would be robustly stable. Finally, the effectiveness of the proposed PID algorithm is examined through experiments on a planar cable driven robot and it is shown that the proposed control structure is able to provide suitable performance in practice.

1. Introduction

Cable driven parallel manipulators (CDPMs) are a special class of parallel robots in which the rigid extensible links are replaced by actuated cables. In a CDPM the end-effector is connected to the base by a number of active cables, and by controlling the cables length the end-effector is moved toward the desired position and orientation. Based on this structure, cable driven robots have some advantages compared to that of conventional parallel robots. Replacing rigid links by cables inaugurates many potential applications such as very large workspace robots [1,2], high speed manipulation [3], handling of heavy materials [4], cleanup of disaster areas [5], access to remote locations, and interaction with hazardous environment [6].

CDPMs can be classified into two types, fully-constrained and under-constrained [5,7,8]. In the fully-constrained type cables can create any wrench by pulling on the end-effector [9] or equivalently, for a given set of cable lengths the end-effector cannot be moved in position and orientation [5,10]. To fully constrain a CDPM the number of cables driving the end-effector must be at least one greater than the number of robot degree of freedoms. According to aforementioned facts, a wrench-closure pose of a CDPM is a pose at which the end-effector is fully-constrained by the cables. Based on this definition, wrench-closure workspace of a CDPM can be defined as the set of wrench-closured poses [11]. The wrench-closure workspace only depends on the geometry of the mechanism [8,12]. The cable robots to be discussed in this paper are of fully-constrained type and it is assumed that the motion control is in the wrench-closure workspace.

Replacing rigid links by cables, however, introduces many new challenges in the study of CDPMs which are quite different from that of conventional robots. Unlike the rigid links, cables can only apply tensile forces and therefore they shall be kept in tension in the whole workspace of the robot and as soon as the cables become slack, the structure of the cable robot collapses [13]. Due to above mentioned physical limitation, well-known control theories cannot be used directly for CDPMs and they must be modified to provide positive tension for the cables. In the field of parallel robots, there are many researches on dynamics and control aspects [14–16]. However, in comparison with the large amount of articles published on the control of conventional robots only few has been published on the control of cable driven robots. With assumption of massless rigid string model for the cables some of the control schemes which have been used for conventional robots may be adapted for CDPMs. Lyapunov based control [3,17], computed torque method [17,18], sliding mode [19] and fuzzy plus PI control [20] are some control algorithms being used in the control of CDPMs.

Kawamura et al. have proposed a control algorithm in cable length coordinates using PD controller with gravity compensation and internal forces [3]. The stability of motion is analysed based on Lyapunov theorem and vector closure conditions. Alp and Agrawal used PD control with gravity compensation in task space coordinates and analyzed asymptotic stability based on Lyapunov second

* Corresponding author. Tel.: + 98 21 8406 2321.
E-mail addresses: m.a.khosravi@dena.kntu.ac.ir (M.A. Khosravi), Taghirad@kntu.ac.ir (H.D. Taghirad).

0957-4158/$ - see front matter © 2013 Elsevier Ltd. All rights reserved.
http://dx.doi.org/10.1016/j.mechatronics.2013.12.001

method [17]. Inverse Dynamics Control (IDC) or computed torque technique is another method which is used in [17,18]. In this technique, the actuator forces are calculated to cancel out the effects of nonlinear dynamical terms on the manipulator. Fang et al. used nonlinear feedforward control laws in the cable length coordinates [21]. They proposed optimal tension distribution algorithm to compensate dynamic errors.

But in these studies, the controller structures are usually complex and robust stability analysis of the closed loop system is not investigated. As a consequence, real time implementation of these controllers is not efficient and even may be impractical. Furthermore, exact and accurate information of dynamic equations of the CDPMs is not accessible in practice and only some partial information of the dynamics terms with uncertainties is available. Thus, investigating robust performance of the mechanism and real time implementation issue are of particular importance. Only few studies have been performed systematically relating to these aspects.

The goal of this paper is to develop a theoretical framework for robust position control of CDPMs based on a simple PID controller structure. To develop the idea, modeling uncertainties are taken into account and robust stability of the closed-loop system with proposed control algorithm is performed. According to the unique property of cables that can only pull and not push and in order to ensure that all the cables remain in tension for all maneuvers in their workspace, a corrective term is used in the proposed control algorithm. This term which interpreted as internal forces is obtained based on null space of transposed Jacobian matrix of the robot. In this paper we assume that the motion is within the wrench-closure workspace and as a consequence, for all times, sufficient positive internal forces can be produced such that the cables are kept in tension. Furthermore, it is assumed that in nonlinear dynamic equations of the cable robot all terms are uncertain and only some information about their upper bounds is available. A robust PID controller is proposed to overcome the partly missing knowledge of the robot and to guarantee boundedness of tracking errors. Then, robust stability of the system with proposed control algorithm is analyzed through Lyapunov second method. To confirm the effectiveness of the proposed control algorithm, the proposed control structure is implemented on a planar cable driven robot with four actuated cables as shown in Fig. 1. As shown in this figure, the fixed attachment points are located on the vertices of a rectangle to provide a relatively large workspace of about four square meters.

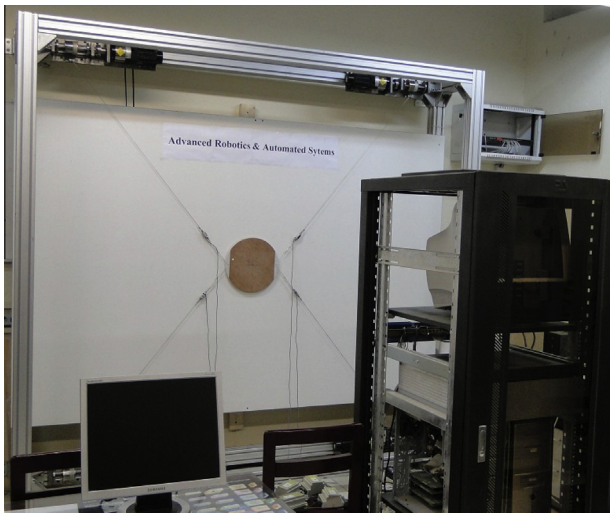

Fig. 1. Prototype of a planar cable driven robot fabricated at K. N. Toosi University of Technology.

The paper is organized as follows. In Section 2 kinematics and dynamics of CDPMs are studied, some properties of dynamic equations are elaborated and the bounds on dynamical terms are determined. Section 3 focuses on the control in which the proposed control scheme is introduced and a method is presented to tune the control gains based on the bounds of dynamical terms. Then, robust stability of the closed loop system is analyzed through Lyapunov direct method. Finally, to show the effectiveness of the proposed control algorithm experimental results on a planar CDPM are discussed in Section 4 and the results are summarized in Section 5.

2. Robot kinematics and dynamics

2.1. Kinematics analysis

Cable driven robot is a closed kinematic chain mechanism whose end-effector is connected to the base by a number of actuated cables. The kinematics notation of a general cable driven parallel robot with n cables is shown in Fig. 2. In this figure $\boldsymbol{l}_i$ is the vector along ith cable and the magnitude of $\boldsymbol{l}_i$ is the same length as the cable. The length of the ith cable is denoted by l_i. $\boldsymbol{S}_i$ denotes the unit vector along the ith cable from the base to the end-effector. A_i and B_i denote the attachment points of the ith cable on the base and the end-effector, respectively. The positions of the attachment points A_i and B_i are represented by vectors $\boldsymbol{a}_i, \boldsymbol{b}_i$, respectively. Obviously, $\boldsymbol{a}_i$ is a constant vector in the base frame F_o and $\boldsymbol{b}_i$ is a constant vector in the end-effector frame F_e. The origin of the end-effector frame F_e is fixed at a reference point P, the center of mass of the end-effector which is used to define the position vector of the end-effector $\boldsymbol{p}$. Based on the kinematics notation defined in Fig. 2 the position of the end-effector may be given by:

$$\boldsymbol{p} = \boldsymbol{a}_i + \boldsymbol{l}_i - \boldsymbol{b}_i \quad (i = 1, 2, \cdots, n) \tag{1}$$

where all vectors are represented in the base frame F_o. As a result

$$l_i^2 = [\boldsymbol{p} - \boldsymbol{a}_i + \boldsymbol{b}_i]^T \cdot [\boldsymbol{p} - \boldsymbol{a}_i + \boldsymbol{b}_i] \tag{2}$$

Differentiate this equation with respect to time, and rewrite it into matrix form as:

$$\dot{\boldsymbol{L}} = \tilde{\boldsymbol{J}}\boldsymbol{t} \tag{3}$$

where

$$\tilde{\boldsymbol{J}} = \begin{bmatrix} \boldsymbol{S}_1 & \boldsymbol{S}_2 & \cdots & \boldsymbol{S}_n \\ \boldsymbol{b}_1 \times \boldsymbol{S}_1 & \boldsymbol{b}_2 \times \boldsymbol{S}_2 & \cdots & \boldsymbol{b}_n \times \boldsymbol{S}_n \end{bmatrix}^T \tag{4}$$

in which $\dot{\boldsymbol{L}} = \left[\dot{l}_1, \dot{l}_2, \cdots, \dot{l}_n\right]^T$ denotes the velocity vector in cable length space and the end-effector twist is denoted by $\boldsymbol{t} = [\dot{\boldsymbol{p}}^T, \boldsymbol{\omega}^T]^T = [\dot{p}_x, \dot{p}_y, \dot{p}_z, \omega_x, \omega_y, \omega_z]^T$. The matrix $\tilde{\boldsymbol{J}}$ is the Jacobian matrix corresponding to the general CDPM, and $\dot{\boldsymbol{p}}$ denotes the velocity vector of point P and $\boldsymbol{\omega}$ denotes the angular velocity of the end-effector.

2.2. Dynamics analysis

For a cable robot the mass of the cables is extremely small compared to the end-effector and can therefore be neglected. Based on the dynamics notation in Fig. 3, when all cables are in tension the equations of motion can be derived using Newton–Euler formulations [22].

$$\begin{bmatrix} m\mathbf{I}_{3\times3} & \mathbf{0}_{3\times3} \\ \mathbf{0}_{3\times3} & \mathbf{I}_P \end{bmatrix} \begin{bmatrix} \ddot{\boldsymbol{p}} \\ \dot{\boldsymbol{\omega}} \end{bmatrix} + \begin{bmatrix} \mathbf{0}_{3\times1} \\ \boldsymbol{\omega} \times \mathbf{I}_P\boldsymbol{\omega} \end{bmatrix} + \begin{bmatrix} -m\boldsymbol{g} \\ \mathbf{0}_{3\times1} \end{bmatrix} = -\tilde{\boldsymbol{J}}^T\boldsymbol{\tau} \tag{5}$$

In this equation, m denotes the mass of the end-effector; $\boldsymbol{I}_P$ denotes the inertia tensor of the end-effector about point P in F_o frame; $\boldsymbol{I}_{3\times3}$ is a 3×3 identity matrix; $\boldsymbol{g}$ denotes the gravity acceleration vector;

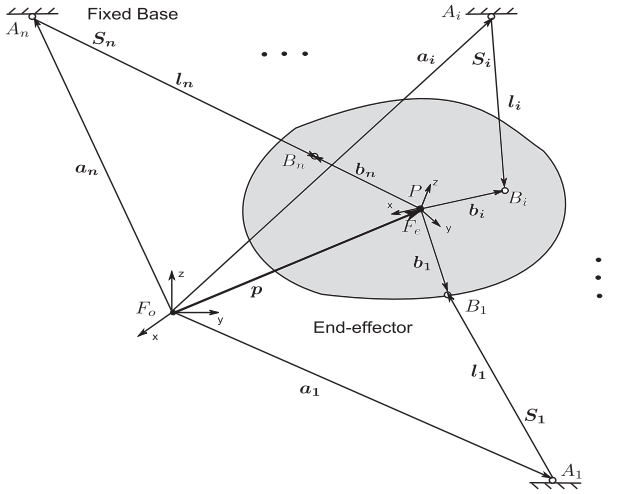

Fig. 2. Schematic of a general CDRPM denoting kinematics notions.

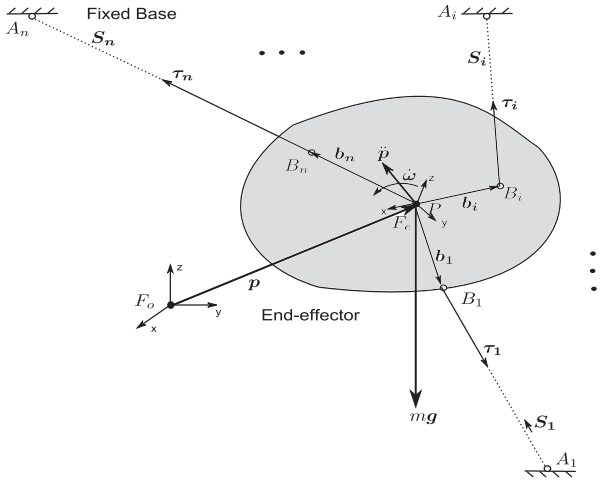

Fig. 3. Schematic of a general CDRPM denoting dynamics notions.

$\boldsymbol{\tau} = [\tau_1, \tau_2, \cdots, \tau_n]$ denotes the vector of cable forces, while scalar τ_i denotes the tension force of the ith cable.

Consider $\boldsymbol{x} = [x_p, y_p, z_p, \alpha, \beta, \gamma]^T$ as generalized coordinates vector, in which $\boldsymbol{\theta} = [\alpha, \beta, \gamma]^T$ denotes the vector of a set of Pitch–Roll–Yaw Euler angles. With this definition the rotation matrix ${}^{F_o}\boldsymbol{R}_{F_e}$ can be written in terms of Pitch-Roll-Yaw Euler angels as:

$$ {}^{F_o}\boldsymbol{R}_{F_e} = \begin{bmatrix} c\beta c\gamma & c\gamma s\alpha s\beta - c\alpha s\gamma & c\alpha c\gamma s\beta + s\alpha s\gamma \\ c\beta s\gamma & c\alpha c\gamma + s\alpha s\beta s\gamma & -c\gamma s\alpha + c\alpha s\beta s\gamma \\ -s\beta & c\beta s\alpha & c\alpha c\beta \end{bmatrix} \tag{6} $$

where s and c represent sin and cos functions, respectively. Furthermore, the angular velocity of the end-effector can be written in the following form,

$$ \boldsymbol{\omega} = \boldsymbol{E}\dot{\boldsymbol{\theta}}, \;\; \dot{\boldsymbol{\theta}} = \left[\dot{\alpha}, \dot{\beta}, \dot{\gamma}\right]^T \tag{7} $$

in which,

$$ \boldsymbol{E} = \begin{bmatrix} \cos(\beta)\cos(\gamma) & -\sin(\gamma) & 0 \\ \cos(\beta)\sin(\gamma) & \cos(\gamma) & 0 \\ -\sin(\beta) & 0 & 1 \end{bmatrix} $$

Thus, one can write

$$ \dot{\boldsymbol{L}} = \boldsymbol{J}\dot{\boldsymbol{x}} \tag{8} $$

in which,

$$ \boldsymbol{J} = \tilde{\boldsymbol{J}} \begin{bmatrix} \boldsymbol{I}_{3\times3} & \boldsymbol{0}_{3\times3} \\ \boldsymbol{0}_{3\times3} & \boldsymbol{E} \end{bmatrix} \tag{9} $$

With this notation, the equations of motion can be written in terms of $\boldsymbol{x}$. By some manipulations these equations may be derived as,

$$ \boldsymbol{M}(\boldsymbol{x})\ddot{\boldsymbol{x}} + \boldsymbol{C}(\boldsymbol{x}, \dot{\boldsymbol{x}})\dot{\boldsymbol{x}} + \boldsymbol{G}(\boldsymbol{x}) = -\boldsymbol{J}^T\boldsymbol{\tau} \tag{10} $$

where

$$ \boldsymbol{M}(\boldsymbol{x}) = \begin{bmatrix} m\boldsymbol{I}_{3\times3} & \boldsymbol{0}_{3\times3} \\ \boldsymbol{0}_{3\times3} & \boldsymbol{E}^T\mathbf{I}_P\boldsymbol{E} \end{bmatrix} \tag{11} $$

$$ \boldsymbol{C}(\boldsymbol{x}, \dot{\boldsymbol{x}})\dot{\boldsymbol{x}} = \begin{bmatrix} \boldsymbol{0}_{3\times1} \\ \boldsymbol{E}^T\{\boldsymbol{I}_P\dot{\boldsymbol{E}}\dot{\boldsymbol{\theta}} + (\boldsymbol{E}\dot{\boldsymbol{\theta}}) \times \boldsymbol{I}_P(\boldsymbol{E}\dot{\boldsymbol{\theta}})\} \end{bmatrix} \tag{12} $$

$$ \boldsymbol{C}(\boldsymbol{x}, \dot{\boldsymbol{x}}) = \begin{bmatrix} \boldsymbol{0}_{3\times3} & \boldsymbol{0}_{3\times3} \\ \boldsymbol{0}_{3\times3} & \boldsymbol{E}^T\mathbf{I}_P\dot{\boldsymbol{E}} + \boldsymbol{E}^T(\boldsymbol{E}\dot{\boldsymbol{\theta}})_\times(\boldsymbol{I}_P\boldsymbol{E}) \end{bmatrix} \tag{13} $$

$$ \boldsymbol{G}(\boldsymbol{x}) = \begin{bmatrix} -m\boldsymbol{g} \\ \boldsymbol{0}_{3\times1} \end{bmatrix} \tag{14} $$

in which, the matrix $(\boldsymbol{E}\dot{\boldsymbol{\theta}})_\times$ is a skew-symmetric matrix defined by the components of the angular velocity vector ω_x, ω_y , and ω_z as

$$ (\boldsymbol{E}\dot{\boldsymbol{\theta}})_\times = \begin{bmatrix} 0 & -\omega_z & \omega_y \\ \omega_z & 0 & -\omega_x \\ -\omega_y & \omega_x & 0 \end{bmatrix} \tag{15} $$

2.3. Properties of the dynamics formulation

In this section some properties of the robot dynamics formulation are investigated. These properties are used in design of control law in order to have simpler and more effective representation. In practice a robot usually experiences friction and disturbance forces during its maneuver. Therefore, the equations of motion can be rewritten as

$$ \boldsymbol{M}(\boldsymbol{x})\ddot{\boldsymbol{x}} + \boldsymbol{C}(\boldsymbol{x}, \dot{\boldsymbol{x}})\dot{\boldsymbol{x}} + \boldsymbol{G}(\boldsymbol{x}) + \boldsymbol{F}_d\dot{\boldsymbol{x}} + \boldsymbol{F}_s(\dot{\boldsymbol{x}}) + \boldsymbol{T}_d = -\boldsymbol{J}^T\boldsymbol{\tau} \tag{16} $$

in which, $\boldsymbol{x}$ denotes the generalized coordinates vector, $\boldsymbol{\tau}$ denotes the vector of cable forces, $\boldsymbol{F}_d$ as the coefficient matrix of viscous friction and $\boldsymbol{F}_s$ as a Coulomb friction term. $\boldsymbol{M}(\boldsymbol{x})$ denotes the mass matrix, $\boldsymbol{C}(\boldsymbol{x}, \dot{\boldsymbol{x}})$ denotes the Coriolis/centripetal matrix, and $\boldsymbol{G}(\boldsymbol{x})$ denotes the gravity vector which are defined in previous section. $\boldsymbol{J}$ is the jacobian matrix of the robot and $\boldsymbol{T}_d$ denotes disturbance which may represent any modeling uncertainty. The robot dynamics may be written as

$$ \boldsymbol{M}(\boldsymbol{x})\ddot{\boldsymbol{x}} + \boldsymbol{N}(\boldsymbol{x}, \dot{\boldsymbol{x}}) = -\boldsymbol{J}^T\boldsymbol{\tau} \tag{17} $$

where,

$$ \boldsymbol{N}(\boldsymbol{x}, \dot{\boldsymbol{x}}) = \boldsymbol{C}(\boldsymbol{x}, \dot{\boldsymbol{x}})\dot{\boldsymbol{x}} + \boldsymbol{G}(\boldsymbol{x}) + \boldsymbol{F}_d\dot{\boldsymbol{x}} + \boldsymbol{F}_s(\dot{\boldsymbol{x}}) + \boldsymbol{T}_d \tag{18} $$

2.3.1. Properties of the mass matrix

Using $\boldsymbol{M}(\boldsymbol{x})$ expression, it can be shown that in spite of uncertainty in the parameters $\boldsymbol{M}(\boldsymbol{x})$ is symmetric, positive definite and bounded from above and below. Boundedness property of $\boldsymbol{M}(\boldsymbol{x})$ implies that

$$ \underline{m}\boldsymbol{I} \leqslant \boldsymbol{M}(\boldsymbol{x}) \leqslant \overline{m}\boldsymbol{I} \tag{19} $$

or

$$ \underline{m} \leqslant \|\boldsymbol{M}(\boldsymbol{x})\| \leqslant \overline{m} \tag{20} $$

where $\boldsymbol{I}$ is the identity matrix and $\underline{m}$ and $\overline{m}$ are positive scalars.

2.3.2. Properties of coriolis and centripetal matrix

From (13) it is clear that dependence on $\boldsymbol{x}$ appears only in terms of sin and cos functions, and therefore $\boldsymbol{C}(\boldsymbol{x}, \dot{\boldsymbol{x}})$ has an upper bound

that is independent of $\boldsymbol{x}$. However this bound is a function of $\dot{\boldsymbol{x}}$. Thus, we can write

$$\|\boldsymbol{C}(\boldsymbol{x},\dot{\boldsymbol{x}})\| \leqslant \xi_c\|\dot{\boldsymbol{x}}\| \tag{21}$$

where ξ_c is a known, positive scalar.

Furthermore, it can be shown that the matrix representing the difference between time derivative of the mass matrix $\boldsymbol{M}(\boldsymbol{x})$ and Coriolis/centripetal Matrix $\boldsymbol{C}(\boldsymbol{x},\dot{\boldsymbol{x}})$ is a skew symmetric matrix [23]. That is,

$$\boldsymbol{z}^T(\dot{\boldsymbol{M}}(\boldsymbol{x}) - 2\boldsymbol{C}(\boldsymbol{x},\dot{\boldsymbol{x}}))\boldsymbol{z} = 0 \tag{22}$$

2.3.3. Properties of gravity vector

According to (14), it is clear that in spite of uncertainty in mass of the end-effector, gravity vector has an upper bound. Thus

$$\|\boldsymbol{G}(\boldsymbol{x})\| \leqslant \xi_g \tag{23}$$

where ξ_g is a known and positive scalar.

2.3.4. Properties of friction terms

Friction terms are complex, and indeed, may be the most contrary terms to describe in the robot dynamics model [24]. Coulomb friction has a functional dependance on $\dot{\boldsymbol{x}}$, although due to eccentricities in power transmissions and other effects, it may depend on the position as well that it is ignored in this paper. Frictions are dissipative and a bound on the friction terms may be assumed by

$$\|\boldsymbol{F}_d\dot{\boldsymbol{x}} + \boldsymbol{F}_s(\dot{\boldsymbol{x}})\| \leqslant \xi_{f0} + \xi_{f1}\|\dot{\boldsymbol{x}}\| \tag{24}$$

It is assumed that ξ_{f0} and ξ_{f1} are known and positive constants.

2.3.5. Properties of the disturbance term

As it is mentioned before, disturbance term may be used to represent any inaccuracy in model dynamics. Therefore, it may be assumed that it is bounded by

$$\|\boldsymbol{T}_d\| \leqslant \xi_t \tag{25}$$

where ξ_t is a known and positive constant.

3. Robust PID control of cable driven robot

In this section considering uncertainties in the robot model a robust PID controller is proposed based on the bounds of dynamical terms of the equations of motion and then its robust stability is analyzed with respect to the model uncertainties. In stability analysis it is assumed that the dynamical terms $\boldsymbol{M}(\boldsymbol{x})$, $\boldsymbol{C}(\boldsymbol{x},\dot{\boldsymbol{x}})$ and other terms are uncertain and there is only some information about their bounds. Furthermore, it is assumed that Jacobian matrix of the manipulator ($\boldsymbol{J}$) cannot be obtained precisely, and therefore we have to use an inaccurate estimated Jacobian matrix $\hat{\boldsymbol{J}}$. The control law is designed based on these bounds and assumptions such that to satisfy some conditions for robust stability.

Recall the dynamic model of system (16) and design a PID controller for $-\hat{\boldsymbol{J}}^T\boldsymbol{\tau}$ by:

$$\boldsymbol{f} = -\hat{\boldsymbol{J}}^T\boldsymbol{\tau} = \boldsymbol{K}_V\dot{\boldsymbol{e}} + \boldsymbol{K}_P\boldsymbol{e} + \boldsymbol{K}_I\int_0^t \boldsymbol{e}(s)ds = \boldsymbol{K}\boldsymbol{y} \tag{26}$$

$\boldsymbol{f}$ is the applied wrench on the end-effector by the cables and

$$\begin{cases} \boldsymbol{e} = \boldsymbol{x}_d - \boldsymbol{x} \\ \boldsymbol{K} = [\boldsymbol{K}_I \quad \boldsymbol{K}_P \quad \boldsymbol{K}_V] \\ \boldsymbol{y} = \left[\int_0^t \boldsymbol{e}^T(s)ds \quad \boldsymbol{e}^T \quad \dot{\boldsymbol{e}}^T\right]^T \end{cases}$$

in which, $\boldsymbol{x}_d$ is the vector of desired trajectory and $\boldsymbol{e}$ denotes the position and orientation errors. According to (26) the proposed PID control is formed in task space and thus to implement the controller it should be mapped onto cable length (joint) space, while satisfies cables tensionability condition.

As it mentioned earlier, in the fully-constrained type of the cable robots redundancy in actuation is necessary. Thus, Jacobian matrix of the mechanism is a non-square matrix and as a result (26) is an under-determined system of equations and has many solutions if $\hat{\boldsymbol{J}}^T\hat{\boldsymbol{J}}$ is invertible. In this case general solution of (26) is,

$$\boldsymbol{\tau} = \overline{\boldsymbol{\tau}} + \boldsymbol{Q}. \tag{27}$$

Here, $\boldsymbol{\tau}$ denotes the vector of tension in the cables and $\overline{\boldsymbol{\tau}}$ is the minimum solution of (26) derived by using the pseudo-inverse of inaccurate transposed Jacobian matrix $\hat{\boldsymbol{J}}^T$ and is given by

$$\overline{\boldsymbol{\tau}} = -\hat{\boldsymbol{J}}(\hat{\boldsymbol{J}}^T\hat{\boldsymbol{J}})^{-1}\left[\boldsymbol{K}_V\dot{\boldsymbol{e}} + \boldsymbol{K}_P\boldsymbol{e} + \boldsymbol{K}_I\int_0^t \boldsymbol{e}(s)ds\right] \tag{28}$$

The vector $\boldsymbol{Q}$ which is used in the control effort to ensure that all cables remain in tension, can be written in the following form

$$\boldsymbol{Q} = \mathbb{N}(\hat{\boldsymbol{J}}^T)\boldsymbol{c} \tag{29}$$

$\mathbb{N}(\hat{\boldsymbol{J}}^T)$ is the null space or kenel of matrix $\hat{\boldsymbol{J}}^T$ and $\boldsymbol{c}$ is a $(n-r)$-dimentional vector, where r is the rank of matrix $\hat{\boldsymbol{J}}^T$ and n is the number of cables. A well known results in the literature on cable robots report that a pose is fully-constrained if and only if the corresponding wrench matrix $\boldsymbol{W}_r$ (in this paper $-\boldsymbol{J}^T$) is of full rank and there exists a positive vector $\boldsymbol{h} > 0$ in the null space of $\boldsymbol{W}_r$ [9]. According to (29), $\boldsymbol{Q}$ is a positive vector and it spans the null space of $\hat{\boldsymbol{J}}^T$ which satisfies

$$\hat{\boldsymbol{J}}^T\boldsymbol{Q} = \boldsymbol{0} \tag{30}$$

$\boldsymbol{Q}$ can be physically interpreted as the vector of *internal forces* and it may increase the stiffness of the system [13]. Based on the aforementioned discussion, tensionability condition is met using the vector of internal forces

$$\boldsymbol{\tau} = \overline{\boldsymbol{\tau}} + \boldsymbol{Q} \geqslant \boldsymbol{0} \tag{31}$$

With this notation, the proposed control scheme is implemented according to Fig. 4. In this paper we assume that the motion is within the wrench-closure workspace and as a consequence, positive internal forces can be produced to keep the cables in tension.

The estimated Jacobian matrix $\hat{\boldsymbol{J}}^T$ is assumed to be bounded by the following upper bounds

$$\|\boldsymbol{I} - \boldsymbol{J}^T\hat{\boldsymbol{J}}^{\dagger}\| \leqslant \delta_1, \quad \|\boldsymbol{J} - \hat{\boldsymbol{J}}\| \leqslant \delta_2 \tag{32}$$

in which, $\hat{\boldsymbol{J}}^{\dagger}$ is the pseudo-inverse of $\hat{\boldsymbol{J}}^T$. Substitute control law $\boldsymbol{\tau}$ denoted by (27) into (16) to get the following relation for the closed-loop system:

$$\dot{\boldsymbol{y}} = \boldsymbol{A}\boldsymbol{y} + \boldsymbol{B}\Delta\boldsymbol{A} \tag{33}$$

in which,

$$\boldsymbol{A} = \begin{bmatrix} \boldsymbol{0} & \boldsymbol{I}_6 & \boldsymbol{0} \\ \boldsymbol{0} & \boldsymbol{0} & \boldsymbol{I}_6 \\ -\boldsymbol{M}^{-1}\boldsymbol{K}_I & -\boldsymbol{M}^{-1}\boldsymbol{K}_P & -\boldsymbol{M}^{-1}\boldsymbol{K}_V \end{bmatrix}$$
$$\boldsymbol{B} = \begin{bmatrix} \boldsymbol{0} \\ \boldsymbol{0} \\ \boldsymbol{M}^{-1} \end{bmatrix} \tag{34}$$

and

$$\Delta\boldsymbol{A} = \boldsymbol{N}(\boldsymbol{x},\dot{\boldsymbol{x}}) + \boldsymbol{M}\ddot{\boldsymbol{x}}_d + (\boldsymbol{I} - \boldsymbol{J}^T\hat{\boldsymbol{J}}^{\dagger})\boldsymbol{f} + (\boldsymbol{J}^T - \hat{\boldsymbol{J}}^T)\boldsymbol{Q}$$

Before stating the stability results, we present the following lemma.

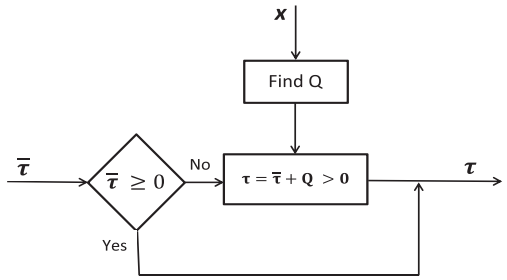

Fig. 4. Internal force control structure.

Lemma 3.1. *Assume that the following properties hold for Lyapunov function of a dynamic system:*

$$\underline{v}\|\boldsymbol{X}\|^2 \leqslant V(\boldsymbol{X}) \leqslant \overline{v}\|\boldsymbol{X}\|^2,$$
$$\dot{V}(\boldsymbol{X}) \leqslant \|\boldsymbol{X}\|(\phi_0 - \phi_1\|\boldsymbol{X}\| + \phi_2\|\boldsymbol{X}\|^2) \tag{35}$$

where $\underline{v}$, $\overline{v}$ *and* ϕ_i $(i = 0, 1, 2)$ *are constants. Given that*

$$d = \frac{2\phi_0}{\phi_1 + \sqrt{\phi_1^2 - 4\phi_0\phi_2}}\sqrt{\frac{\overline{v}}{\underline{v}}} \tag{36}$$

then the system with the initial condition $\boldsymbol{X}_0$ *is uniformly ultimately bounded with respect to* $B(0, d)$*, provided that*

$$\phi_1 > 2\sqrt{\phi_0\phi_1} \tag{37}$$
$$\phi_1^2 + \phi_1\sqrt{\phi_1^2 - 4\phi_0\phi_2} > 2\phi_0\phi_2(1 + \sqrt{\frac{\overline{v}}{\underline{v}}}) \tag{38}$$
$$\phi_1 + \sqrt{\phi_1^2 - 4\phi_0\phi_2} > 2\phi_2\|\boldsymbol{X}_0\|\sqrt{\frac{\overline{v}}{\underline{v}}} \tag{39}$$

where $\|\boldsymbol{X}_0\|$ *denotes the norm of the initial condition.*

Proof. Proof can be found in [25] under 3.1 □

3.1. Stability analysis

To analyze the robust stability of the system consider the following Lyapunov function candidate

$$V(\boldsymbol{y}) = \boldsymbol{y}^T\boldsymbol{P}\boldsymbol{y} \tag{40}$$

in which,

$$\boldsymbol{P} = \frac{1}{2}\begin{bmatrix} \mu\boldsymbol{K}_P + \mu\boldsymbol{K}_I + \mu^2\boldsymbol{M} & \mu\boldsymbol{K}_V + \boldsymbol{K}_I + \mu^2\boldsymbol{M} & \mu\boldsymbol{M} \\ \mu\boldsymbol{K}_V + \boldsymbol{K}_I + \mu^2\boldsymbol{M} & \mu\boldsymbol{K}_V + \boldsymbol{K}_P + \mu^2\boldsymbol{M} & \mu\boldsymbol{M} \\ \mu\boldsymbol{M} & \mu\boldsymbol{M} & \boldsymbol{M} \end{bmatrix}$$

and μ is a positive scalar and $\mu < 0.5$. Now if we assume diagonal gain matrices for PID controller,

$$\boldsymbol{K}_P = k_P\boldsymbol{I}, \quad \boldsymbol{K}_V = k_V\boldsymbol{I}, \quad \boldsymbol{K}_I = k_I\boldsymbol{I}$$

Then we can conclude on the positive definiteness of matrix $\boldsymbol{P}$ by the following lemma.

Lemma 3.2. *Assume the following inequalities hold:*

$$0 < \mu < 0.5 \tag{41}$$
$$s_1 = \mu(k_P - k_V) - (1 - \mu)k_I - \mu\overline{m} > 0 \tag{42}$$
$$s_2 = k_P - k_I - \mu\overline{m} > 0 \tag{43}$$

Then $\boldsymbol{P}$ *is positive definite and satisfies the following inequality (Rayleigh–Ritz):*

$$\underline{\lambda}(\boldsymbol{P})\|\boldsymbol{y}\|^2 \leqslant V(\boldsymbol{y}) \leqslant \overline{\lambda}(\boldsymbol{P})\|\boldsymbol{y}\|^2 \tag{44}$$

in which,

$$inf(\underline{\lambda}(\boldsymbol{P})) = min\{\frac{1 - 2\mu}{2}\underline{m}, \frac{s_1}{2}, \frac{s_2}{2}\}$$
$$sup(\overline{\lambda}(\boldsymbol{P})) = max\{\frac{1 + 2\mu}{2}\overline{m}, \frac{s_3}{2}, \frac{s_4}{2}\}$$

and

$$s_3 = \mu(k_P + k_v) + (1 + \mu)k_I + (1 + 2\mu)\mu\overline{m}$$
$$s_4 = \mu\overline{m}(1 + 2\mu) + 2\mu k_V + k_P + k_I$$

$\underline{m}$ *and* $\overline{m}$ *are defined before in* (20).

Proof. Proof is based on Gershgorin theorem and is similar to that in [26] when $\alpha_1 = \alpha_2 = \mu$. □

Now when $\boldsymbol{P}$ is positive definite then we can conclude on the negative definiteness of the Lyapunov function (40).

$$\dot{V}(\boldsymbol{y}) = \boldsymbol{y}^T(\boldsymbol{A}^T\boldsymbol{P} + \boldsymbol{P}\boldsymbol{A} + \dot{\boldsymbol{P}})\boldsymbol{y} + 2\boldsymbol{y}^T\boldsymbol{P}\boldsymbol{B}\Delta\boldsymbol{A} = -\boldsymbol{y}^T\boldsymbol{H}\boldsymbol{y}$$
$$+ \frac{1}{2}\boldsymbol{y}^T\begin{bmatrix}\mu\boldsymbol{I}\\ \mu\boldsymbol{I}\\ \boldsymbol{I}\end{bmatrix}\dot{\boldsymbol{M}}[\,\mu\boldsymbol{I} \quad \mu\boldsymbol{I} \quad \boldsymbol{I}\,]\boldsymbol{y} + \boldsymbol{y}^T\begin{bmatrix}\mu\boldsymbol{I}\\ \mu\boldsymbol{I}\\ \boldsymbol{I}\end{bmatrix}\Delta\boldsymbol{A}$$
$$+ \frac{1}{2}\boldsymbol{y}^T\begin{bmatrix}\boldsymbol{0} & \mu^2\boldsymbol{M} & \mu^2\boldsymbol{M}\\ \mu^2\boldsymbol{M} & 2\mu^2\boldsymbol{M} & (\mu^2 + \mu)\boldsymbol{M}\\ \mu^2\boldsymbol{M} & (\mu^2 + \mu)\boldsymbol{M} & 2\mu\boldsymbol{M}\end{bmatrix}\boldsymbol{y}$$

Referring to (22),

$$\boldsymbol{z}^T\dot{\boldsymbol{M}}\boldsymbol{z} = 2\boldsymbol{z}^T\boldsymbol{C}\boldsymbol{z}$$

therefore,

$$\dot{V}(\boldsymbol{y}) = -\boldsymbol{y}^T\boldsymbol{H}\boldsymbol{y} + \frac{1}{2}\boldsymbol{y}^T\begin{bmatrix}\mu\boldsymbol{I}\\ \mu\boldsymbol{I}\\ \boldsymbol{I}\end{bmatrix}(\boldsymbol{C} + \boldsymbol{C}^T)[\,\mu\boldsymbol{I} \quad \mu\boldsymbol{I} \quad \boldsymbol{I}\,]\boldsymbol{y} + \boldsymbol{y}^T\begin{bmatrix}\mu\boldsymbol{I}\\ \mu\boldsymbol{I}\\ \boldsymbol{I}\end{bmatrix}\Delta\boldsymbol{A}$$
$$+ \frac{1}{2}\boldsymbol{y}^T\begin{bmatrix}\boldsymbol{0} & \mu^2\boldsymbol{I} & \mu^2\boldsymbol{I}\\ \mu^2\boldsymbol{I} & 2\mu^2\boldsymbol{I} & (\mu^2 + \mu)\boldsymbol{I}\\ \mu^2\boldsymbol{I} & (\mu^2 + \mu)\boldsymbol{I} & 2\mu\boldsymbol{I}\end{bmatrix}\begin{bmatrix}\boldsymbol{M} & \boldsymbol{0} & \boldsymbol{0}\\ \boldsymbol{0} & \boldsymbol{M} & \boldsymbol{0}\\ \boldsymbol{0} & \boldsymbol{0} & \boldsymbol{M}\end{bmatrix}\boldsymbol{y}$$

where

$$\boldsymbol{H} = \begin{bmatrix}\mu k_I\boldsymbol{I} & \boldsymbol{0} & \boldsymbol{0}\\ \boldsymbol{0} & (\mu k_P - \mu k_V - k_I)\boldsymbol{I} & \boldsymbol{0}\\ \boldsymbol{0} & \boldsymbol{0} & k_V\boldsymbol{I}\end{bmatrix}$$

Thus,

$$\dot{V}(\boldsymbol{y}) \leqslant -\gamma\|\boldsymbol{y}\|^2 + \lambda_1\|\boldsymbol{C}\|\|\boldsymbol{y}\|^2 + \mu^{-1}\lambda_1\|\boldsymbol{y}\|\|\Delta\boldsymbol{A}\| + \lambda_2\overline{m}\|\boldsymbol{y}\|^2$$

in which,

$$\gamma = min\{\mu k_I, \mu(k_P - k_V) - k_I, k_V\}$$

In spite of uncertainties in dynamic terms, from dynamics formulation properties we may conclude that

$$\begin{aligned}
\underline{m} \leqslant \boldsymbol{M} &\leqslant \overline{m}\\
\|\boldsymbol{C}(\boldsymbol{x}, \dot{\boldsymbol{x}})\| &\leqslant \xi_c\|\dot{\boldsymbol{x}}\| = \xi_c\|\dot{\boldsymbol{x}}_d - \dot{\boldsymbol{x}} - \dot{\boldsymbol{x}}_d\|\\
&\leqslant \xi_c\|\dot{\boldsymbol{e}}\| + \xi_c\|\dot{\boldsymbol{x}}_d\| \quad \leqslant \quad \beta_3 + \beta_4\|\boldsymbol{y}\|\\
\|\boldsymbol{G}(\boldsymbol{x})\| &\leqslant \xi_g\\
\|\boldsymbol{N}(\boldsymbol{x}, \dot{\boldsymbol{x}})\| &\leqslant \beta_0 + \beta_1\|\boldsymbol{y}\| + \beta_2\|\boldsymbol{y}\|^2\\
\|(\boldsymbol{I} - \boldsymbol{J}^T\hat{\boldsymbol{J}}^{\dagger})\boldsymbol{f}\)\| &\leqslant \|(\boldsymbol{I} - \boldsymbol{J}^T\hat{\boldsymbol{J}}^{\dagger})\|\|\boldsymbol{f}\| \quad \leqslant \quad \delta_1\xi_f\|\boldsymbol{y}\|\\
\|(\boldsymbol{J} - \hat{\boldsymbol{J}})^T\boldsymbol{Q}\| &\leqslant \xi_Q
\end{aligned}$$

By using these inequalities one can rewrite $\dot{V}(\boldsymbol{y})$ as

$$\dot{V}(\boldsymbol{y}) \leqslant \|\boldsymbol{y}\|(\xi_0 - \xi_1\|\boldsymbol{y}\| + \xi_2\|\boldsymbol{y}\|^2) \tag{45}$$

in which,

$$\xi_0 = \mu^{-1}\lambda_1\beta_0 + \mu^{-1}\lambda_1\lambda_3\overline{m} + \mu^{-1}\lambda_1\xi_Q$$
$$\xi_1 = \gamma - \lambda_1\beta_3 - \lambda_2\overline{m} - \mu^{-1}\lambda_1\beta_1 - \delta_1\xi_f \quad (46)$$
$$\xi_2 = \lambda_1\beta_4 + \mu^{-1}\lambda_1\beta_2$$

where

$$\lambda_1 = \lambda_{max}(\mathbf{Q}_1),\ \ \lambda_2 = \lambda_{max}(\mathbf{Q}_2),\ \ \lambda_3 = sup\|\ddot{\boldsymbol{x}}_d\|$$

and λ_{max} denotes the maximum eigenvalue of the matrix. Furthermore,

$$\mathbf{Q}_1 = \begin{bmatrix} \mu^2\mathbf{I} & \mu^2\mathbf{I} & \mu\boldsymbol{I} \\ \mu^2\mathbf{I} & \mu^2\mathbf{I} & \mu\boldsymbol{I} \\ \mu\mathbf{I} & \mu\mathbf{I} & \boldsymbol{I} \end{bmatrix}$$

$$\mathbf{Q}_2 = \frac{1}{2}\begin{bmatrix} \mathbf{0} & \mu^2\mathbf{I} & \mu^2\boldsymbol{I} \\ \mu^2\mathbf{I} & 2\mu^2\mathbf{I} & (\mu^2+\mu)\boldsymbol{I} \\ \mu^2\mathbf{I} & (\mu^2+\mu)\mathbf{I} & 2\mu\boldsymbol{I} \end{bmatrix}$$

According to the result obtained so far, we can prove the stability of the error system based on the following theorem.

Theorem 3.1. *The error system (33) is stable of the form of Uniformly Ultimately Bounded (UUB), if ξ_1 is chosen large enough.*

Proof. According to Eqs. (44) and (45) and Lemma (3.1) if the following conditions hold, the system is UUB stable. The conditions are:

$$\xi_1 > 2\sqrt{\xi_0\xi_2} \quad (47)$$

$$\xi_1^2 + \xi_1\sqrt{\xi_1^2 - 4\xi_0\xi_2} > 2\xi_0\xi_2\left(1 + \sqrt{\frac{\bar{\lambda}(\boldsymbol{P})}{\underline{\lambda}(\boldsymbol{P})}}\right) \quad (48)$$

$$\xi_1 + \sqrt{\xi_1^2 - 4\xi_0\xi_2} > 2\xi_2\|\boldsymbol{y}_0\|\sqrt{\frac{\bar{\lambda}(\boldsymbol{P})}{\underline{\lambda}(\boldsymbol{P})}}. \quad (49)$$

These conditions can be simply met by making ξ_1 large enough. Recall that $\xi_1 = \gamma - \lambda_1\beta_3 - \lambda_2\overline{m} - \mu^{-1}\lambda_1\beta_1 - \delta_1\xi_f$ and $\gamma = min\{\mu k_I, \mu(k_P - k_V) - k_I, k_V\}$, then it can be seen that for any given $0 < \mu < 0.5$, the inequalities (41) and (42) and above mentioned inequalities can be satisfied by suitable choice of PID control gains. □

Remark 3.1. The inequalities (41)–(43) and (47)–(49) form a constructive and conservative algorithm for suitable choice of gains in PID controller.

Remark 3.2. By choosing PID control gains properly, the stabiliy of uniformly ultimate boundeness holds in any finite region of the state space.

This proof reveals an important aspect of the proposed controller law. This aspect that can be concluded from this analysis is robust stability of the closed-loop system in presence of modeling uncertainties. Since the unmodeled but bounded dynamics of the system is systematically encapsulated in the system model (as stated in Eqs. (20)–(25)), the only influence that this impose on the stability is the respective bounds on the controller gains depicted in conditions derived from Lemma 3.2 and Theorem 3.1. At the next section some experimental results are given to verify the effectiveness of the proposed control in practice.

4. Experimental results

4.1. Experimental setup

In order to verify the effectiveness of the proposed method, the robust PID controller is applied to a planar CDPM illustrated in Fig. 1. This manipulator consists of four cable driven actuators with three degrees of freedom planar motion, which is under investigation for high speed and wide workspace applications. The manipulator end-effector has a mass of $m = 2.5$ kg with a variation of 0.5 kg payload. The actuators are located on the vertices of a rectangle with dimension of 2.24 m × 2.1 m. Furthermore, a special design is used in the cable winches by which the attachment points of the robot are kept fixed. As it is shown in Fig. 5, this is accomplished by moving the cable drum along its axis with a pitch equal to the cable width. Furthermore, two touching ball bearings are used to guide the cable toward the end-effector. The block diagram of control system setup is shown in Fig. 6. The host computer serves as the user interface and enables the user to edit and modify control structure and parameters. The target computer is a real time processing unit in which QNX operating system is used and performs real time execution of the control algorithm and real time communication with I/Os. RT-LAB software is used with Simulink to define models in real time environment. RT-LAB is designed to automate the execution of control law for the controllers built in Simulink, in a real time multiprocessing environment [27]. A number of PCI input/output boards were integrated with the RT-LAB and Simulink to create a real time control system.

4.2. Cable robot dynamic model

According to (13) and (16) by neglecting friction terms the equations of motion for planar CDPM can be written in the following form

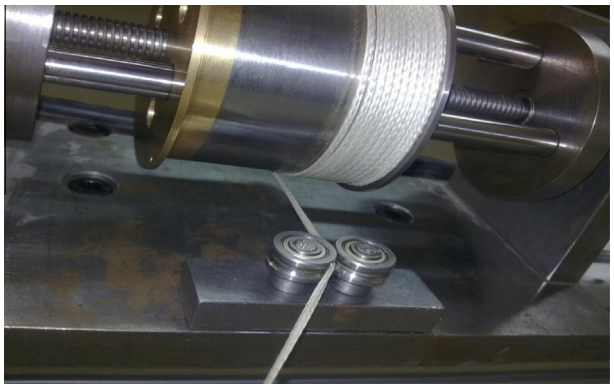

Fig. 5. The system of cable winch.

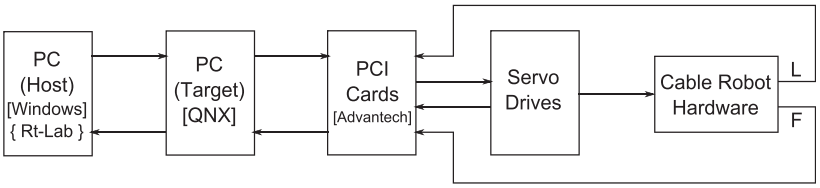

Fig. 6. Control system setup.

Table 1
Position of the cable attachment points.

Attachment points on the base in global frame (m)	Attachment points on the end-effector in local frame (m)
A_1 (−1.12, 1.05)	B_1 (−0.155, 0)
A_2 (1.12, 1.05)	B_2 (0.155, 0)
A_3 (−1.12, −1.05)	B_3 (−0.155, 0)
A_4 (1.12, −1.05)	B_4 (0.155, 0)

Table 2
Inertial parameters of the planar cable robot.

Parameter	Symbol	Value
End-effector mass	m	2.5 ± 0.5 kg
End-effector inertia	I_z	0.1 ± 0.02 kg m^2
Gear ratio	N	50
Gravity Acceleration	g	9.8 m/s^2
Drum radius	r	3.5 cm

$$\boldsymbol{M}\ddot{x} + \boldsymbol{G} + \boldsymbol{T}_d = -\boldsymbol{J}^T\boldsymbol{\tau} \tag{50}$$

where $\boldsymbol{M}$ is the inertia matrix for the mechanism, $\boldsymbol{G}$ is the vector of gravity terms, $\boldsymbol{T}_d$ is the vector of disturbance terms that may be used to represent any inaccuracy in model dynamics and $\boldsymbol{J}$ denotes the Jacobian matrix of the robot. According to (11) and (14)

$$\boldsymbol{M} = \begin{bmatrix} m & 0 & 0 \\ 0 & m & 0 \\ 0 & 0 & I_z \end{bmatrix} \quad \boldsymbol{G} = \begin{bmatrix} 0 \\ mg \\ 0 \end{bmatrix}$$

All geometrical and mechanical parameters of the cable robot are given in Tables 1, and 2.

Based on this structure, bounding norms can be written as

$$\|\boldsymbol{C}(\boldsymbol{x}, \dot{\boldsymbol{x}})\| = 0$$
$$\overline{m} = 3, \quad \underline{m} = 2$$
$$\overline{I}_z = 0.12, \quad \underline{I}_z = 0.08$$
$$\xi_g \leqslant 30$$

Furthermore, To consider the effects of uncertainties in design procedure of the controller, it is assumed that $\xi_t \leqslant 5$. These bounds are used to synthesize the PID control based on conditions derived from Lemma 3.2 and Theorem 3.1. According to these results PID control gains $k_P = 10,000, k_V = 3000, k_I = 1000$ are chosen to satisfy the stability conditions. These gains are used for the experiments and the proposed control algorithm which uses internal forces concept is implemented based on (27).

4.3. Control structure

To have a desirable performance in position and orientation tracking, servo drives should accurately provide the required tensions in the cables according to the proposed control algorithm. In other words, the applied tensions on the end-effector should be the outputs of the proposed algorithm according to (27). This requirement necessitates to have ideal torque sources as the actuators. In practice, however, the actuator drivers suffer from a number of limitations, and cannot perform as ideal torque sources. In order to overcome this shortcoming, cascade control scheme is implemented in the experiments. The cascade control strategy uses two feedbacks, namely the outer loop and the inner loop as shown in Fig. 7. In this figure $\boldsymbol{L}$ and $\boldsymbol{F}$ denote vectors of cables length and cables tension, respectively.

The main goal of the outer loop, which consists of the proposed PID controller, is to control the position and orientation of the end-effector. Inputs of this controller are the position and orientation errors vector and its outputs are the required cable tensions. In the inner loop, the desired tensions are compared to the actual tensions measured by the load cells located near the end-effector attachment points. TLL500 from Transducer Techniques is used to measure the cable tensions in the setup. The proposed controller is implemented using RT-LAB software. The equations of forward kinematics are solved by CFSQP[1] routine [28] implemented as an s-function in Simulink to derive Cartesian position $\boldsymbol{x} = (x, y, \phi)$ from encoders information $\boldsymbol{L}$ in real time.

4.4. Results

The first set of experiments aims to generate two disjointed linear motions in translation and rotation. In x direction, it is considered to move the end-effector from the origin to $[0.25\text{ m}, 0, 0]^T$. In ϕ direction it is considered to rotate the end-effector from its central position to $[0, 0, \frac{\pi}{6} rad]^T$. Furthermore, a more challenging circular profile is considered in the next experiments, to track a circular path of 0.2 m about the central position.

For the first experiment, suppose that the home position for the end-effector is $\boldsymbol{x} = [0, 0, 0]^T$ in SI units and the desired end-effector position and orientation is $\boldsymbol{x}_d = [0.25\text{ m}, 0, 0]^T$. The results of implementation using proposed PID control (26) in companion to the required $\boldsymbol{Q}$ which ensures that all the cables are in tension, are given in Fig. 8. The controller gains are selected in the feasible stability region of the system considering modeling uncertainty bounds as it was mentioned in previous subsection, as $k_P = 10,000, k_V = 3000, k_I = 1000$. As it is seen in this figure, position and orientation outputs track the desired values very well and the steady state errors are very small and in order of 10^{-3}, while as it is shown in Fig. 9 all cables are in tension for the whole maneuver. The prescribed uniformly ultimately bounded tracking error for the control structure is verified in all three directions in this experiment.

In the next experiment, suppose that the desired orientation of the end-effector is $\boldsymbol{x}_d = [0, 0, \frac{\pi}{6} rad]^T$, while the same controller gains are considered. The experimental results are given in Fig. 10. As it is observed, tracking performance is very suitable and the position errors in x and y directions are small and in order of 10^{-3}. Furthermore, as it is shown in Fig. 11, it is observed that all tensions in the cables for this test are also positive.

To investigate the robustness of the proposed controller another test with maximum mass of the end-effector $m = 3$ kg and $\boldsymbol{T}_d = 0.1\boldsymbol{G}$ is performed. As it is shown in Fig. 12, in spite of uncertainties in the dynamics of the manipulator the desired trajectory $\boldsymbol{x}_d = [0.25\text{ m}, 0, 0]^T$ is suitably tracked and the steady state errors can be ignored. Comparing Fig. 12 to Fig. 8 shows that the proposed control algorithm is able to robustly stabilize the system in presence of modeling uncertainties.

For the circular profile, the end-effector is commanded to move from origin and track a circular path with radius of 0.2 meter in 10 s, while attempting to maintain $\phi = 0$ in all time. The reference Cartesian positions for this experiment are $x = 0.2\cos(0.2\pi t)u_s(t - 2.5)$ and $y = 0.2\sin(0.2\pi t)u_s(t)$ where $u_s(t)$ denotes unit step function. Figs. 13 and 14 show the reference and actual circle and

[1] C code for Feasible Sequential Quadratic Programming.

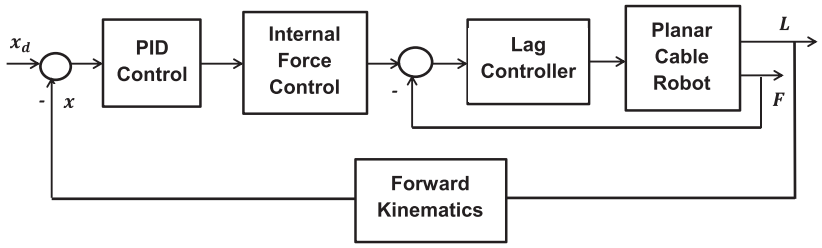

Fig. 7. Cascade control block diagram.

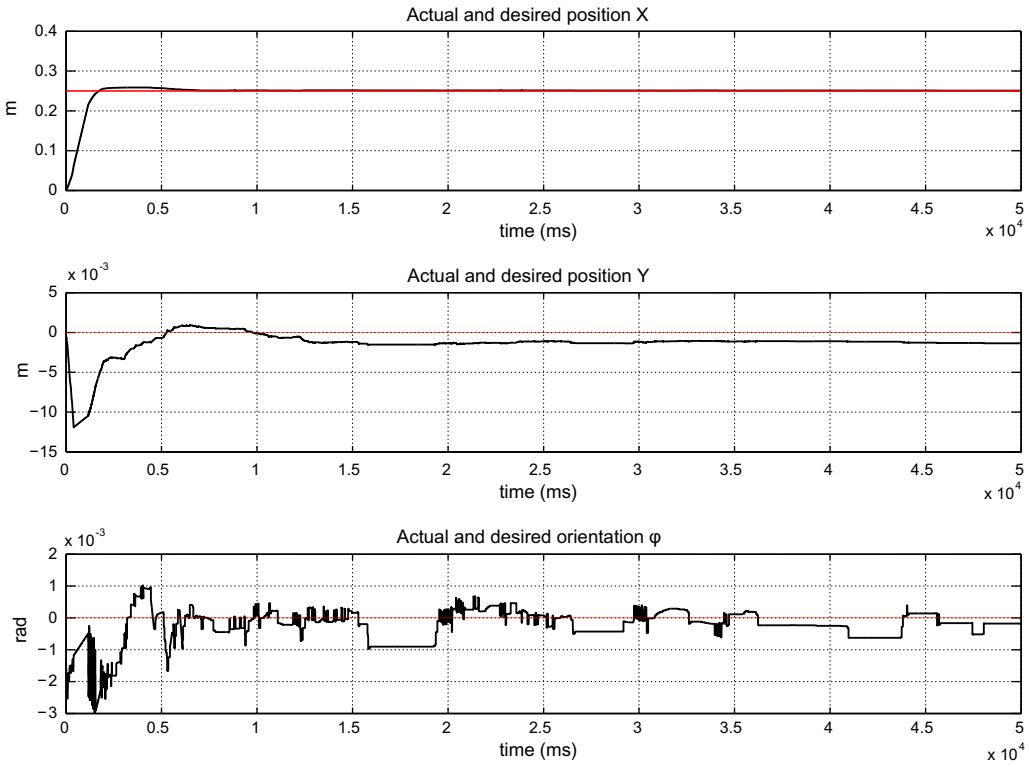

Fig. 8. Implementation results showing the actual and desired position and orientation of the end-effector for $\boldsymbol{x}_d = [0.25\ \text{m}, 0, 0]^T$.

deviation of ϕ from its zero desired value. It can be seen that the proposed PID control scheme is capable to perform such maneuver, while the absolute positioning errors are relatively small. As it is seen in Fig. 14, orientation error in this test is very small and in order of 10^{-3}. There are some potential sources of error in these experiments which are under current improvement. One issue is the friction and backlash in the gearing transmission of the actuators and other uncertainties that are not taken into account. Furthermore, as explained before, actual position and orientation of the end-effector are not directly measured and are computed by forward kinematics solution. This leads to a finite error in the computations which may lead to the final positioning error of the system. Furthermore, the elasticity of the cables is simply neglected in this analysis, which may lead to positioning errors, especially at high speed maneuvers.

To verify the repeatability of the cable robot another experiment is performed. Repeatability of the cable robot is considered by repeating performance of a circular trajectory of the end-effector. In this experiment, the trajectory is considered eight turns for a circle with radius of 0.2 meter, while attempting to maintain zero orientation. Fig. 15 shows the performance of the robot in this experiment. As it is seen in this figure the repeatability performance of the robot is far better than absolute positioning of the end effector.

From the above experimental results, it may be concluded that, although the proposed controller has a simple structure, it can achieve a suitable control performance and has high robustness against uncertainties.

5. Conclusions

This paper addresses the issues of dynamic analysis and control of fully-constrained cable robots. According to unique property of cables that can only apply tensile forces, and in order to ensure that all the cables are in tension for all maneuvers in their workspace, a corrective term based on null space of the Jacobian matrix is used in companion with the proposed PID algorithm. In the design of the proposed PID controller it is assumed that in dynamic equations of cable robot all terms are uncertain and only some information about their upper bounds is available. A Robust PID controller is proposed to overcome partial knowledge of robot, and to

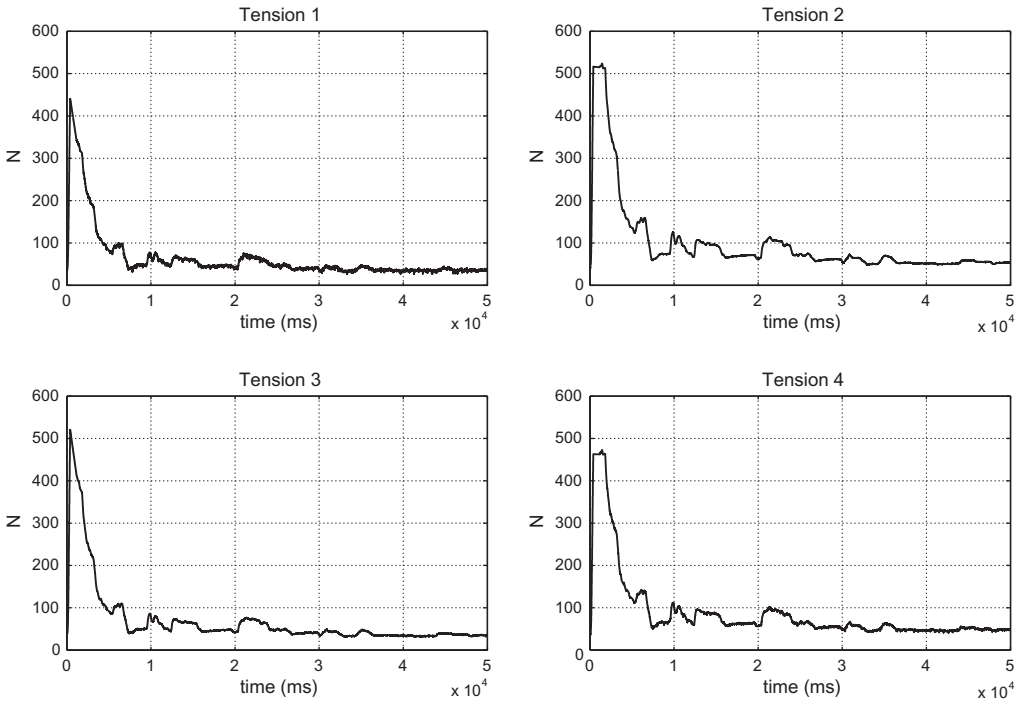

Fig. 9. Implementation results showing the cables tension for $\boldsymbol{x}_d = [0.25\ \text{m}, 0, 0]^T$.

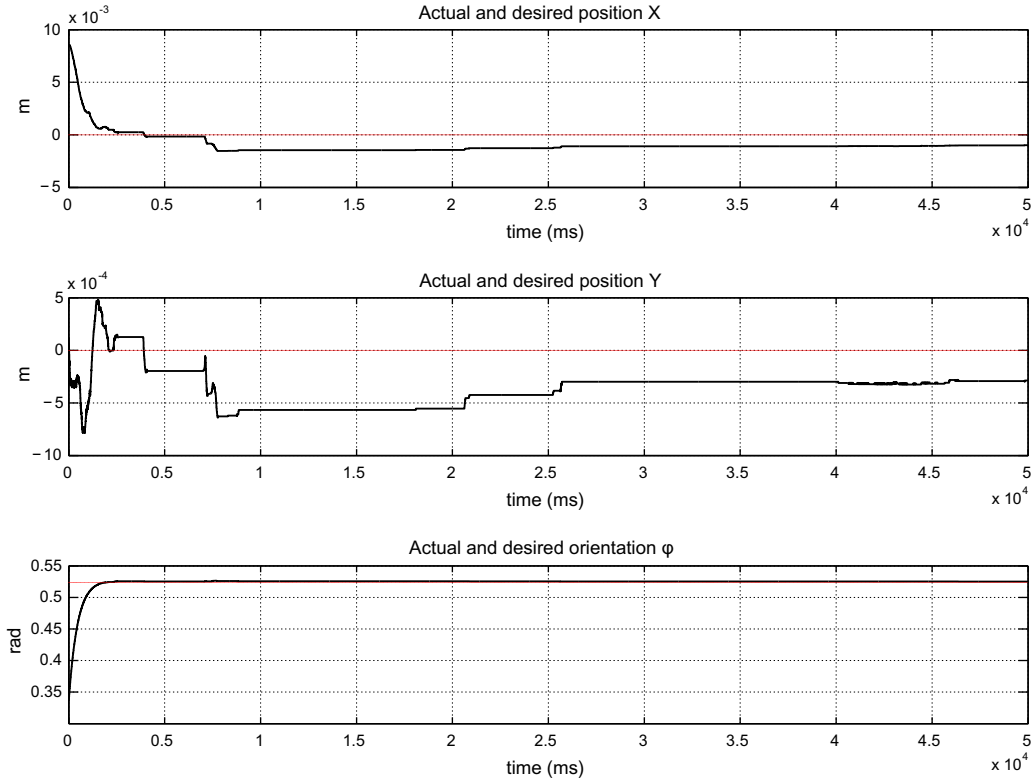

Fig. 10. Implementation results showing the actual and desired position and orientation of the end-effector for $\boldsymbol{x}_d = [0, 0, \frac{\pi}{6} rad]^T$.

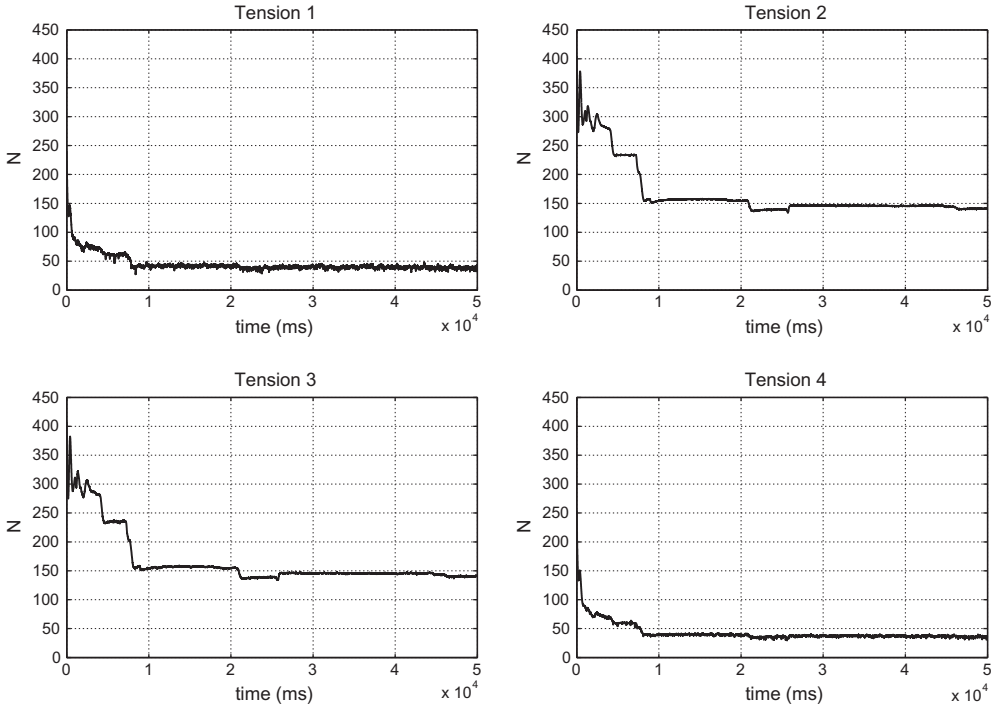

Fig. 11. Implementation results showing the cables tension for $\boldsymbol{x}_d = [0, 0, \frac{\pi}{6} rad]^T$.

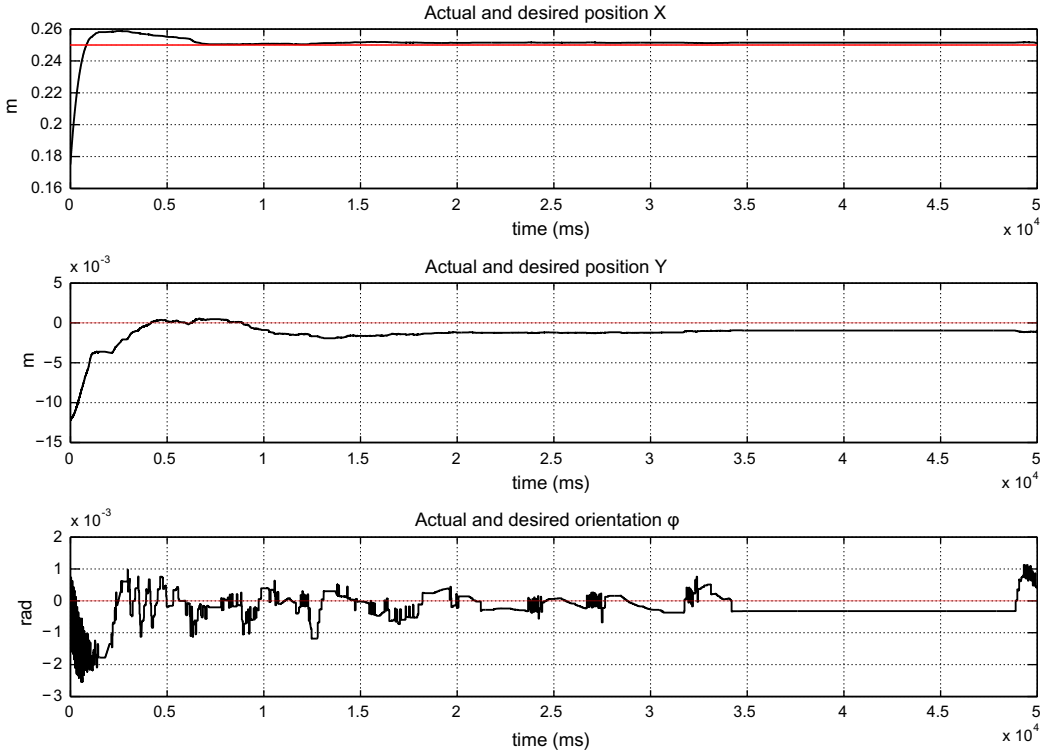

Fig. 12. Suitable tracking performance for the system with uncertainties.

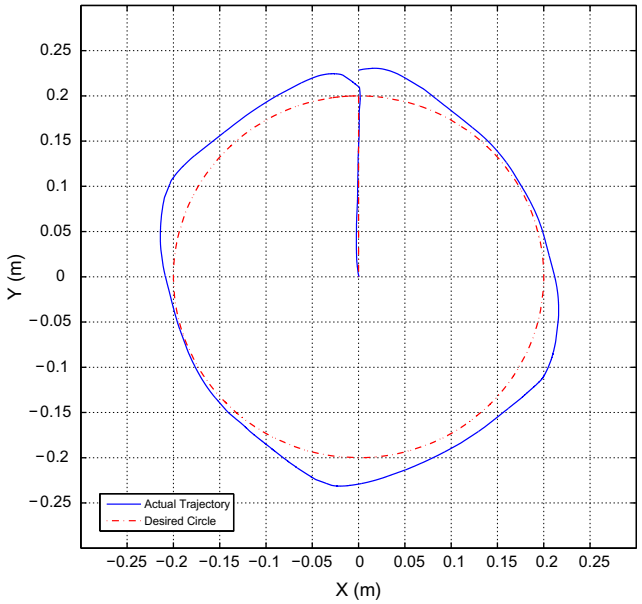

Fig. 13. Implementation results showing circular trajectory generation by the end-effector.

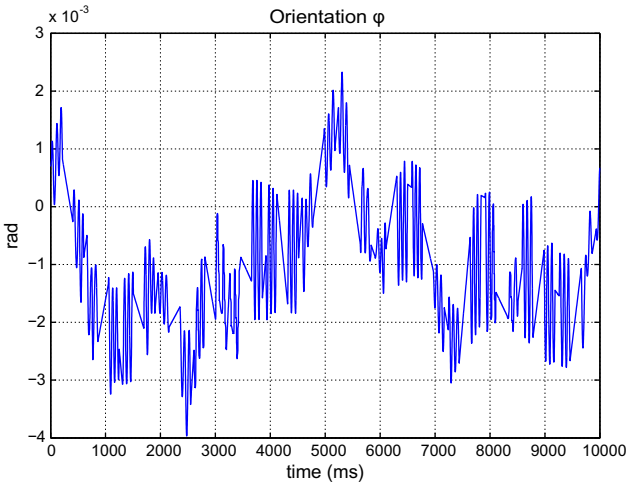

Fig. 14. Implementation results showing the rotation ϕ during circular trajectory generation.

guarantee boundedness of tracking errors. Finally, to show the effectiveness of the proposed algorithm several experiments on a three degrees of freedom planar cable robot are performed with different desired trajectories and suitable tracking performance of the closed loop system is reported.

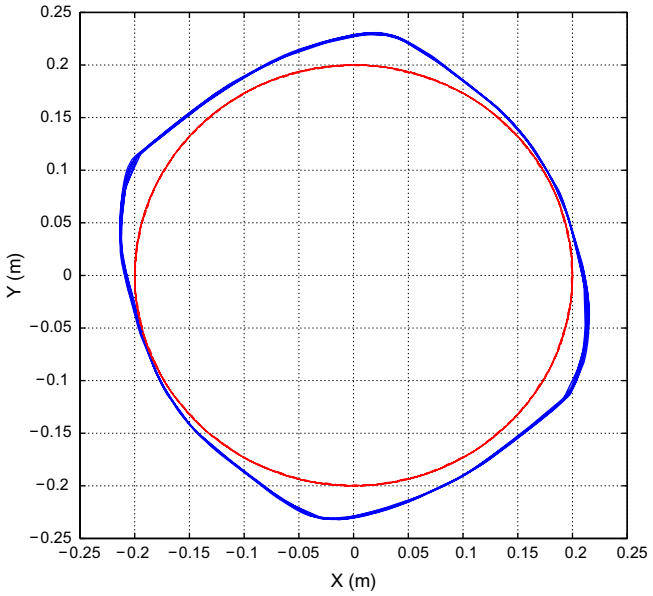

Fig. 15. Implementation results showing the repeatability of the cable robot.

References

[1] Taghirad HD, Nahon M. Kinematic analysis of a macro–micro redundantly actuated parallel manipulator. Adv Rob 2008;22(6-7):657–87.
[2] Cone L. Skycam: an aerial robotic camera system. Byte 1985(10):122–32.
[3] Kawamura S, Kino H, Won C. High-speed manipulation by using parallel wire-driven robots. Robotica 2000;18(3):13–21.
[4] Bostelman R, Albus J, Dagalakis N, Jacoff A. Applications of the NIST robocrane. In: Proceedings of the 5th international symposium on robotics and manufacturing; 1994. p. 403–10.
[5] Roberts R, Graham T, Lippitt T. On the inverse kinematics, statics, and fault tolerance of cable-suspended robots. J Rob Syst 1998;15(10):649–61.
[6] Riechel A, Bosscher P, Lipkin H, Ebert-Uphoff I. Concept paper: cable-driven robots for use in hazardous environments. In: Proceedings of 10th int. topical meet. robot remote syst. hazardous environ. Gainesville; 2004. p. 310–17.
[7] Bosscher PM. Disturbance robustness measures and wrench-feasible workspace generation techniques for cable-driven manipulators, Ph.D. Thesis. Georgia Institute of Technology; 2004.
[8] B Lim W, Yang G, H Yeo S, Mustafa SK. A generic force-closure analysis algorithm for cable-driven parallel manipulators. Mech Mach Theory 2011;46(9):1265–75.
[9] Gouttefarde M. Characterizations of fully constrained poses of parallel cable-driven robots: a review. Proc ASME Int Des Eng Tech Conf 2008:3–6.
[10] Bosscher PM, Riechel AT, Ebert-Uphoff I. Wrench-feasible workspace generation for cable-driven robots. IEEE Trans Rob 2006;22(5):890–902.
[11] Gouttefarde M, Gosselin C. Analysis of the wrench-closure workspace of planar parallel cable-driven mechanisms. IEEE Trans Rob 2006;22(3):434–45.
[12] Pham CB, Yeo SH, Yang G, Kurbanhusen MS, Chen IM. Force-closure workspace analysis of cable-driven parallel mechanisms. Mech Mach Theory 2006;41(1):53–69.
[13] Behzadipour S, Khajepour A. Stiffness of cable-based parallel manipulators with application to stability analysis. J Mech Des 2006;128(1):303–10.
[14] Wu J, Wang J, Wang L, Li T. Dynamics and control of a planar 3-DOF parallel manipulator with actuation redundancy. Mech Mach Theory 2009;44(4):835–49.
[15] Hui C, Yiu-Kuen Y, Zexiang L. Dynamics and control of redundantly actuated parallel manipulators. IEEE/ASME Trans Mech 2003;8(4). 483491.
[16] Wang J, Wu J, Wang L, You Z. Dynamic feed-forward control of a parallel kinematic machine. Mechatronics 2009;19(3):313–24.
[17] Alp A, Agrawal S. Cable suspended robots: feedback controllers with positive inputs. Proc Am Control Conf 2002:815–20.
[18] Williams RL, Gallina P, Vadia J. Planar translational cable direct driven robots. J Rob Syst 2003;20(3):107–20.
[19] Ryoek S, Agrawal S. Generation of feasible set points and control of a cable robot. IEEE Trans Rob 2006;22(3):551–8.
[20] Zi B, Duan B, Du J. Dynamics modeling and active control of a cable-suspended parallel robot. Mechatronics 2008;18:1–12.
[21] Fang S, Franitza D, Torlo M, Bekes F, Hiller M. Motion control of a tendon-based parallel manipulator using optimal tension distribution. IEEE/ASME Trans Mech 2004;9(3):561–8.
[22] Diao X, Ma O. Vibration analysis of cable-driven parallel manipulators. Multibody Syst Dyn 2009;21:347–60.
[23] Merlet JP. Parallel robots. Springer; 2006.
[24] Armstrong-Hélouvry B, Dupont P, De Wit CC. A survey of models, analysis tools and compensation methods for the control of machines with friction. Automatica 1994;30(7):1083–138.
[25] Qu Z, Dawson DM. Robust tracking control of robot manipulators. IEEE Press; 1996.
[26] Qu Z, Dorsey J. Robust PID control of robots. Int J Rob Automat 1991;6(4):228–35.
[27] RT-LAB version 8 User Guide., Opal-RT Company, 2005.
[28] Lawrence C, Zhou JL, Tits AL. User's Guide for CFSQP version 2.0: A C code for solving constrained nonlinear optimization problems, generating iterates satisfying all inequality constraints. Technical Report, Institute for systems Research, University of Maryland, TR-94-16; 1994.